Int. J. Ind. Chem. 2026; 17(1): 51-61

International Journal of Industrial Chemistry (IJIC)

https://doi.org/10.57647/ijic.2026.1701.06

Research Article

In Vitro Delivery of Silica Nanoparticle Encapsulated Silymarin for Pharmaceutical Application with High Efficiency and Low Toxicity

Maryam Hasanzadeh[1], Maryam Khavarpour[1,*], Ali Akbar Moghadamnia[2], Maedeh Mohammadi[3]

[1] *Department of Chemical Engineering, Am.C., Islamic Azad University, Amol, Iran*
[2] *Neuroscience Research Center, Health Research Institute, Babol University of Medical Sciences, Babol, Iran*
[3] *Biotechnology Research Laboratory, Faculty of Chemical Engineering, Babol Noshirvani University of Technology, Babol, Iran*

[*] **Corresponding authors:** maryamkhavarpour58@iau.ac.ir

Article History:

Received:
18 January 2026

Revised:
15 February 2026

Accepted:
04 March 2026

Published in Issue:
31 March 2026

Abstract

Silymarin is the natural bioactive component of milk thistle plant, Silybum marianum (L.) Gaertn with several health effects and valuable therapeutic properties. As a hepatoprotective drug, its biological applications are restricted because of its poor solubility in aqueous environments. This paper presents a study to develop a Silymarin-loaded silica nanoparticle system with enhanced bioavailability and water solubility. Synthesized silica nanoparticles were characterized using XRF, FTIR, Zeta potential, SEM and AFM. They exhibit a quasi-spherical morphology and the average particle size was estimated to be approximately 55 nm. Release study of free and loaded Silymarin in PBS (pH 7.4) and citric acid buffer (pH 5.5) shows enable slow and controlled release of Silymarin. Furthermore, the cellular toxicity was assessed using the MTT method by studying the cell survival rates of MCF-7, Hep-G$_2$, and fibroblast cells. The results showed that Silymarin loaded on silica nanoparticles, compared to free silymarin, could more effectively reduce the activity and growth of Hep-G2 and MCF-7 cells even at lower concentrations of Silymarin.

Keywords: Cellular toxicity; Drug delivery; Release; Silymarin; Silica nanoparticles

Cite this article: Hasanzadeh M, Khavarpour M, Moghadamnia A A, Mohammadi M. In Vitro Delivery of Silica Nanoparticle Encapsulated Silymarin for Pharmaceutical Application with High Efficiency and Low Toxicity. Int. J. Ind. Chem. 2026; 17(1): 51-61. https://doi.org/10.57647/ijic.2026.1701.06

1. Introduction

Creating and developing controlled drug delivery systems has ushered in substantial drug administration and permeability progress, leading to notable strides in disease treatment [1, 2]. Silica nanoparticles have gained attention due to their compatibility and ease of drug formulation [3]. Their high surface-to-volume ratio, high reactivity, structural stability, regular channels, and non-toxic nature make them a versatile platform for drug loading. Given the volume of cavities and high porosity, various biological substances can be accommodated within these cavities [4]. Pursuing innovative drug delivery systems, focusing on controlled and enhanced drug delivery and permeability, has ushered in remarkable progress in disease treatment [5]. Rice husk is a notable source of silica production, boasting a higher silica content than other agricultural residues. The composition of rice husk includes approximately 35% cellulose, 25% hemicellulose, 20% lignin, and 17% ash [6].

Silica nanoparticles can be obtained from rice husk through methods such as sol-gel [7, 8], chemical vapor deposition [9], micro-emulsion processes [10], combustion synthesis [11], microwave-assisted methods [12], and more. Most of these methods are complex and require significant energy and time for production. Using thermal decomposition could result to silica nanoparticles with a purity exceeding 95% from rice husk in an amorphous state. These nanoparticles possess higher specific surface area, reactivity, and activity than their crystalline form [13].

Rice husk can be also used as an economical source for the production of silica, as it addresses the problems associated with the disposal of rice bran and the environmental pollution caused by it [14]. In 2001, Dela et al. employed various methods to obtain higher levels of silica from rice husk. The study was conducted at temperatures ranging from 400 to 700 °C, with time intervals of 1, 3, and 6 h. The results indicated that a temperature of 700 °C over 6 h produced 95% silica powder. This research demonstrated that the initial washing of rice husk with one of the solvents (HCl, HNO_3, H_2SO_4, NaOH, or $NaOH_4$) prior to thermal treatment within the temperature range of 500 to 1400 °C, with varying time intervals, could be effective in removing more metal impurities and producing completely white ash from silica [15].

In another study, Real et al. confirmed that by burning rice bran at 600 °C under atmospheric condition and washing it with acid, silica powder with 99.9% purity was obtained [16]. Alshatwi et al. conducted a research study in 2015, where SiO2 nanoparticle were achieved by burning rice husk and pre-treating with hydrochloric acid (HCl) at temperatures of 500, 600, and 700 °C.

The biocompatibility of the produced nanoparticles was examined using toxicity analysis on normal fibroblast cells. The results showed that these nanoparticles were biocompatible and could be a suitable alternative to synthetic SiO2 nanoparticle in the food and pharmaceutical industries [17].

Silymarin has gained significant attention in treating various diseases, such as liver diseases, cardiovascular conditions, diabetes, kidney disorders, pasoriasis, various types of cancers, and chemotherapy due to its antioxidant properties and high bioavailability [18].

The chemical formula of Silymarin is ($C_{25}H_{22}O_{10}$) [19], and it is found in the extract of seeds of milk thistle plant. The dry seed extract of this plant contains 1% to 4% Silymarin, which includes flavonoids such as silybin A and B (33.4%), silydianin (3.5%), silychristin (12.9%), and isosilybin (8.35%) [20, 21].

Silybin is the most crucial compound in Silymarin (80-70%), known for its unique antioxidant properties, and recognizes as a liver protector [19, 22, 23]. Due to the low solubility of Silymarin in aqueous environments, its use is limited, and typically, this drug is loaded onto various nanocarriers to enhance its solubility [24, 25]. In 2017, Ji-Soo Lee et al. demonstrated that nanocapsulation of Silymarin increased its solubility and antibacterial properties [26].

In 2019, Sara S. Nasr et al., by investigating the parameters affecting liver function in living organisms, showed that oral administration of Silymarin loaded onto mesoporous silica nanoparticles at a dose of 250 mg/kg significantly outperformed free Silymarin. Over an extended period, this formulation exhibited no apparent toxicity and had a notable increase in solubility [27].

Considering the previous studies, this research aims to enhance Silymarin's bioavailability and solubility, in view of its extensive application in treating various diseases, including liver diseases.

Here, thermal decomposition method was chosen to synthesize silica nanoparticles and load silymarin as a drug onto the synthesized nanoparticles. Release studies in buffer phosphate were studied.

In addition, cellular assays were conducted on Hep-G_2, fibroblasts, and MCF-7 cells. Various analysis, including XRF, FTIR, AFM, HPLC, SEM, and Zeta potential, were also performed.

2. Materials and Methods

2.1. Materials

Ethanol (96%), hydrochloric acid (HCl), potassium hydroxide (KOH), disodium hydrogen phosphate (Na2HPO4), dihydrogen phosphate (H2PO4), sodium dihydrogen phosphate dihydrate (NaH2PO4.2H2O), rice husk, Silymarin 98% (S0292-Sigma, Aldrich), Hep-G2 cells, MCF-7 fibroblasts, dialysis bag, diethyl ether, and tetrazolium salt 3-(4,5-dimethylthiazol-2-yl)-2,5-diphenyltetrazolium bromide (MTT).

2.2. Synthesis of silica nanoparticles by thermal decomposition method

For doing experiments, 110 g of rice husk obtained from rice huller factory in Mazandaran, located in Amol city, were initially washed, dried at room temperature, and then mixed with 12N hydrochloric acid (46 mL) and deionized water (505 mL) for 30 min.

Subsequently, the mixture was placed in an autoclave at 121°C for 45 min. After autoclaving, the mixture was repeatedly washed with distilled water until it reached a neutral pH. After this step, the mixture was left in the oven at 50°C for 24 h.

The dried rice husk were then subjected to thermal decomposition in a muffle furnace at 700°C for 1 h to convert into silica [15, 28, 29]. Fig. 1a shows the schematic procedure for synthesize of silica nanoparticles.

10.57647/ijic.2026.1701.06

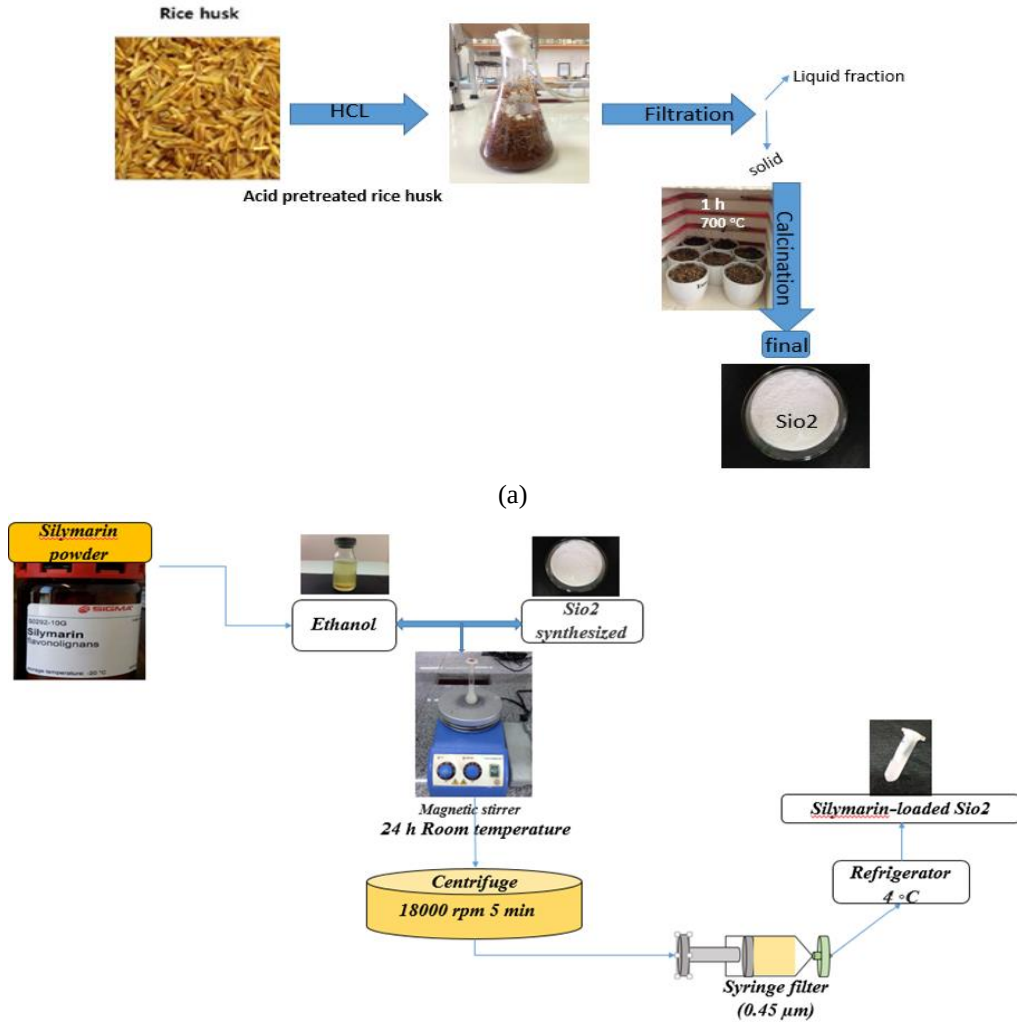

Figure 1. Schematic representation of (a) Synthesis of silica nanoparticle by thermal decomposition and (b) Silymarin loading onto synthesized silica nanoparticle

2.3. Loading Silymarin onto synthesized silica nanoparticles

The process of loading Silymarin onto synthesized silica nanoparticles, as depicted in Fig. 1b, is outlined in this section. Silica nanoparticles synthesized in different weight percentages were employed as carrier to achieve optimal physicochemical properties for Silymarin drug at various concentrations inside glass vials. Subsequently, these silica carriers were placed on a stirrer for 24 h at room temperature to allow adsorption process.

After the specified time had elapsed, the resulting suspension was transferred to appropriate Falcon tubes and centrifuged at 18,000 rpm for 5 min at refrigerated condition (4°C). The supernatant (clear solution) was separated from the obtained sediment, and the centrifugation process was repeated three times under the previous conditions.

Finally, the clear solution was transferred to a spectrophotometer to determine the specific adsorption value. The determination of drug loading percentage and encapsulation efficiency was conducted utilizing the subsequent mathematical formulation [30, 31]. Eqs. (1) and (2) determined Silymarin loading and entrapment.

$$\text{Drug loading} = \frac{\text{weight of Silymarin in silica nanoparticle}}{\text{weight of Silymarin + silica nanoparticle}} \times 100 \quad (1)$$

$$\text{Encapsulation efficiency} = \frac{\text{Weight of Silymarin in silica nanoparticle}}{\text{Weight of initial Silymarin}} \times 100 \quad (2)$$

2.4. Silymarin release in phosphate buffer at various pH

To investigate the pattern of Silymarin release, drug release tests were conducted at 1, 2, 3, 4, 24, 48, 72, and 96 h at a temperature of 37°C. Silymarin release from the synthesized silica nanoparticle under in vitro conditions was examined using the dialysis bag method. In brief, 5 mg of silica nanoparticles loaded with Silymarin was enclosed within a dialysis bag (Molecular weight cutoff

10.57647/ijic.2026.1701.06

(Mw): 14 kDa) and wholly immersed in 40 mL of phosphate-buffered saline (PBS, pH 7.4).

Subsequently, 2 mL of the solution outside of the dialysis bag was withdrawn as a sample at scheduled time points, and 2 mL of fresh PBS was added. The release studies were repeated three times. All the above-mentioned procedures were also investigated in PBS with a pH of 5.5 to evaluate the drug's sensitivity to pH.

As a control, the release of free Silymarin in PBS with pH of 7.4 and 5.5 was evaluated using the same method. The quantity of Silymarin in the samples was determined at a wavelength of 275 nm using a UV spectrophotometer. The release percentages of Silymarin were calculated as below [32].

$$\text{Release}(\%) = \frac{\text{weight of Silymarin(mg)}}{\text{Total weight of Silymarin (mg)}} \times 100$$

The fractional weight of released Silymarin at a specific time, "t," and the denominator, which is the fractional amount of total Silymarin present in the dialysis bag before the onset of release, are calculated.

2.5. Evaluation of cellular toxicity on living cell lines of Hep-G$_2$, fibroblasts, and MCF-7

MCF-7, Hep-G$_2$, and fibroblast cells were cultured in RPMI medium containing 10% heat-inactivated fetal bovine serum (FBS), 100 U/mL penicillin, and 100 µg/mL streptomycin at 37°C with 5% CO_2. The cells were passaged three times a week, and their purity and growth rate were regularly examined.

For the MTT assay, cells were seeded in 96-well plates. The impact of synthesized silica nanoparticles and released drugs on living cells was evaluated using the MTT method. MCF-7 and Hep-G$_2$ cells were used as cancer cells, while fibroblasts served as normal cells. Silymarin was employed as the free drug, and synthesized silica nanoparticles without drug and drug-loaded nanoparticles were examined to assess cellular toxicity [33].

At the end of the incubation period, 3-[4,5-dimethylthiazol-2-yl]-2,5-diphenyltetrazolium bromide (MTT) was added to each well at a concentration of 0.5 mg/mL, and incubation continued for 4 h. Living cells with functional mitochondria can convert MTT to formazan.

After removing the supernatant from each well, a specific amount of dimethyl sulfoxide (DMSO) was added. Plates were further incubated for 10 minutes, and their absorbance was measured using a microplate reader. The number of living cells was calculated using following equation [34].

$$\text{Cell Viability } \% = \frac{\text{mean OD of treated cells}}{\text{mean OD of control cells}} \times 100$$

2.6. Investigation of influential parameters on drug loading performance on silica nanoparticles

In order to create optimal conditions and enhance efficiency in the loading process while preventing drug and synthesized nanoparticle loss, the influential parameters affecting adsorption were examined, which are detailed below.

2.6.1. *Effect of the weight ratio of Silymarin/silica nanoparticle*

Initially, 5 mg of Silymarin was dissolved as the solvent in 100 mL of ethanol. Subsequently, various weight ratios of Silymarin/silica nanoparticles were placed on a stirrer at a temperature of 25°C.

Then, the suspension of each sample was centrifuged at 18,000 rpm for 5 minutes at refrigerator temperature. The clear supernatant solutions were transferred to a UV device for absorbance measurement. The percentage of encapsulation and loading for each sample was calculated and reported.

2.6.2. *Optimal concentration of Silymarin*

After determining the optimal weight ratio of Silymarin/silica nanoparticle, various concentrations of the Silymarin and solvent were prepared. Subsequently, using the mentioned method and calculating encapsulation and drug loading, the optimal concentration of Silymarin was selected for further analysis.

2.7. Characterization of silica nanoparticles

X-ray Fluorescence analysis (XRF) was employed as the analytical method to ascertain the composition of elements and metal oxides within the synthesized silica nanoparticles. Fourier Transform Infrared Spectroscopy (FTIR) was conducted utilizing the WQF-510A model, China to study functional groups within the synthesized silica and the combination of silica and Silymarin. The analytical spectrum encompassed the range of 400-4000 cm^{-1}. Using SEM analysis (QUANTA 200 made by FEI company, USA), the morphology of the samples was examined. The size and zeta potential of synthesized nanoparticles were also assessed using DLS (Dynamic Light Scattering).

To delve into the size distribution of nanoparticles, Atomic Force Microscopy (AFM) was harnessed as the investigative tool. A diluted nanoparticle solution, with a concentration of 1000 mg/L, was meticulously prepared in methanol, serving as the solvent of choice. Subsequently, several drops of the resulting suspension were meticulously deposited onto a glass slide and desiccated under ambient air conditions.

Table 1. Effect of weight ratio of Silymarin/silica nanoparticle on encapsulation efficiency and drug loading percentage

Silymarin/silica nanoparticle (w/w)	%EE	%DL
1/2	36.405	18.20
1/5	40.405	8.08
1/10	44.6036	4.46
1/20	43.302	2.17
1/100	45.378	0.071

EE= Encapsulation efficiency, DL= Drug loading

Table 2. Effect of Silymarin weight on encapsulation efficiency and drug loading percentage

Silymarin/silica nanoparticle (w/w)	EE%	DL %
1/10	44.60±4.62	4.60±0.26
2/10	75.63±4.83	15.30±0.55
3/10	88.32±3.60	26.86±0.62
4/10	83.02±3.41	32.32±0.78
5/10	71.44±2.43	37.16±0.70

EE= Encapsulation efficiency, DL= Drug loading

After that, the AFM apparatus was employed to generate a graphical representation of the particle size distribution.

The quantification of Silymarin was carried out by utilizing High-Performance Liquid Chromatography (HPLC). The instrumental setup featured a C18 column measuring 4.6 × 250 mm, a pre-column, a pumping system, and a UV detector.

The mobile phase employed was a mixture of acetonitrile and water in a 90:10 ratio, with a flow rate set at 1.5 mL/min. The column temperature was meticulously maintained at 30°C, and a sample injection volume of 20 µL was judiciously chosen.

The initial step involved the construction of a standard curve for Silymarin, with concentrations spanning 2.5, 5, 10, and 20 ppm. The resulting standard curve was subsequently employed to determine the correlation coefficient (R^2). Following this, the injection of the sample into the HPLC system was performed, enabling the quantification of Silymarin concentration through the calculation of the area under the curve concerning the established standard curve, thereby facilitating the determination of Silymarin concentration within the unknown sample.

3. Results and Discussion

The successful synthesis and appropriate performance of a drug nanocarrier depend on various factors, such as the proper structure of the nanocarrier, particle morphology, size, zeta potential (ζ), encapsulation efficiency (%EE), drug loading percentage (%DL), controlled release, and particle toxicity. Accurate evaluation of these factors will significantly contribute to a proper understanding of the performance of the synthesized nanocarrier.

3.1. Effect of weight ratio of Silymarin/silica nanoparticle on encapsulation efficiency (%EE) and drug loading percentage (%DL)

The effect of weight ratio of Silymarin/silica nanoparticle with constant weight of Silymarin on encapsulation efficiency and drug loading percentage is shown in Table 1. The results show that the encapsulation percentage was increased by increasing the weight ratio of Silymarin/silica nanoparticle from 1/2 to 1/10 in constant weight of Silymarin. This may happen because the less amount of Silymarin is wasted and Silymarin has a greater chance of being trapped.

Then, the percentage of encapsulation has been decreased. However, upper than the weight ratio of Silymarin/silica nanoparticle of 1/10, since the Silymarin weight is constant, encapsulation efficiency was decreased. At the weight ratio of 1/10, the encapsulation efficiency and Silymarin loading were obtained to be 44.60% and 4.46%, respectively.

3.2. The effect of Silymarin weight on encapsulation efficiency (%EE) and drug loading percentage (%DL)

After obtaining the optimal weight ratio, the effect of increasing the amount of silymarin drug on encapsulation efficiency and loading percentage was investigated. The results are reported in Table 2. The highest encapsulation efficiency corresponds to the ratio of 3/10 was equal to 88.32%. The drug loading percentage for this ratio was calculated to be 26.86%. Beyond the point of 3/10, the encapsulation efficiency has decreased, which can be attributed to the saturation of silica nanoparticle.
These results were used for the subsequent steps of the experiments.

3.3. Characterization of silica nanoparticles

Weight percentage (%) of elements and metal oxides for synthesized silica nanoparticles is as below:
Na_2O, 0.91; MgO, 0.69, Al_2O_3,1.39; Sio_2, 95.48; P_2O_5, 0.48; Cl, 0.47; K_2O, 0.1; CaO, 0.14; Fe_2O_3, 0.14.

As seen, weight percentage of sio_2 was obtained 95.48%. The synthesized silica nanoparticles was used for further in-depth investigation. The morphology and size distribution of synthesized nanoparticles, assessed using AFM, are depicted in Fig. 2.

The synthesized nanoparticles exhibit a quasi-spherical morphology. The size of nanoparticles evaluated through atomic force microscopy was predominantly reported in the 47-50 nm range, whereas the size of

10.57647/ijic.2026.1701.06

Silymarin-loaded nanoparticles fell within the 50-57 nm range. Particle size, surface charge, surface modifications, hydrophobicity, and more factors influence the targeting of nanoparticles.

Among these factors, particle size and size distribution are significant in determining the interaction of nanoparticles with cellular membranes and drug penetration through various biological barriers related to tissues, target cells, and the bloodstream circulation system. Additionally, for the detection and removal of nanoparticles by macrophages, the size of nanoparticles is the first and most critical parameter under investigation. The surface charge of particles is another crucial factor influencing the delivery and release of loaded therapeutic agents within nanoparticles. These factors depend on various aspects, including particle aggregation and formation in the bloodstream, interaction with membranes, blood circulation patterns, lifespan, and elimination by the body's immune system. Surface charge, often measured as zeta potential, is an essential indicator of nanocarrier stability.

Fig. 3 presents the size and surface charge of nanoparticles. According to the DLS, the average size of nanoparticles was approximately 40.7 nm, with the largest size being around 44.07 nm. A zeta potential of -27.2 mV was also reported. Based on conducted studies, the surface charge of silica falls within the range of -20 to -30 mV [35]. The size and zeta potential of Silymarin-loaded silica nanoparticle were more significant, with a size of approximately 50.9 nm.

The zeta potential of Silymarin-loaded silica nanoparticle was reported as -23.5 mV. This can suggest the potential for an extended circulation time of nanocarriers within the body. Using SEM, the average size of the synthesized silica nanoparticles was calculated to be approximately 42 nm, confirming their nanoscale nature, as depicted in Fig. 4a.

These particles exhibited a perfectly spherical shape and a uniform distribution. In Fig. 4b, SEM images of the Silymarin-loaded silica nanoparticles is presented. The average particle size was estimated to be approximately 55 nm. This increase in size can be attributed to the entrapment of Silymarin within the silica matrix, resulting in successful loading. Quantitative analysis of loaded Silymarin was performed using HPLC.

Fig. 5 a and b represent the HPLC chromatograms of standard Silymarin (10 ppm) and loaded Silymarin after purification using the described method. To determine the purity of Silymarin, a 10-ppm sample was prepared and injected into HPLC, comparing the results with a 10-ppm standard Silymarin sample. Silymarin purity was determined as below:

$$Silymarin\ purity(\%) = \frac{The\ value\ obtained\ by\ HPLC\ (\text{ppm})}{10\ ppm}$$

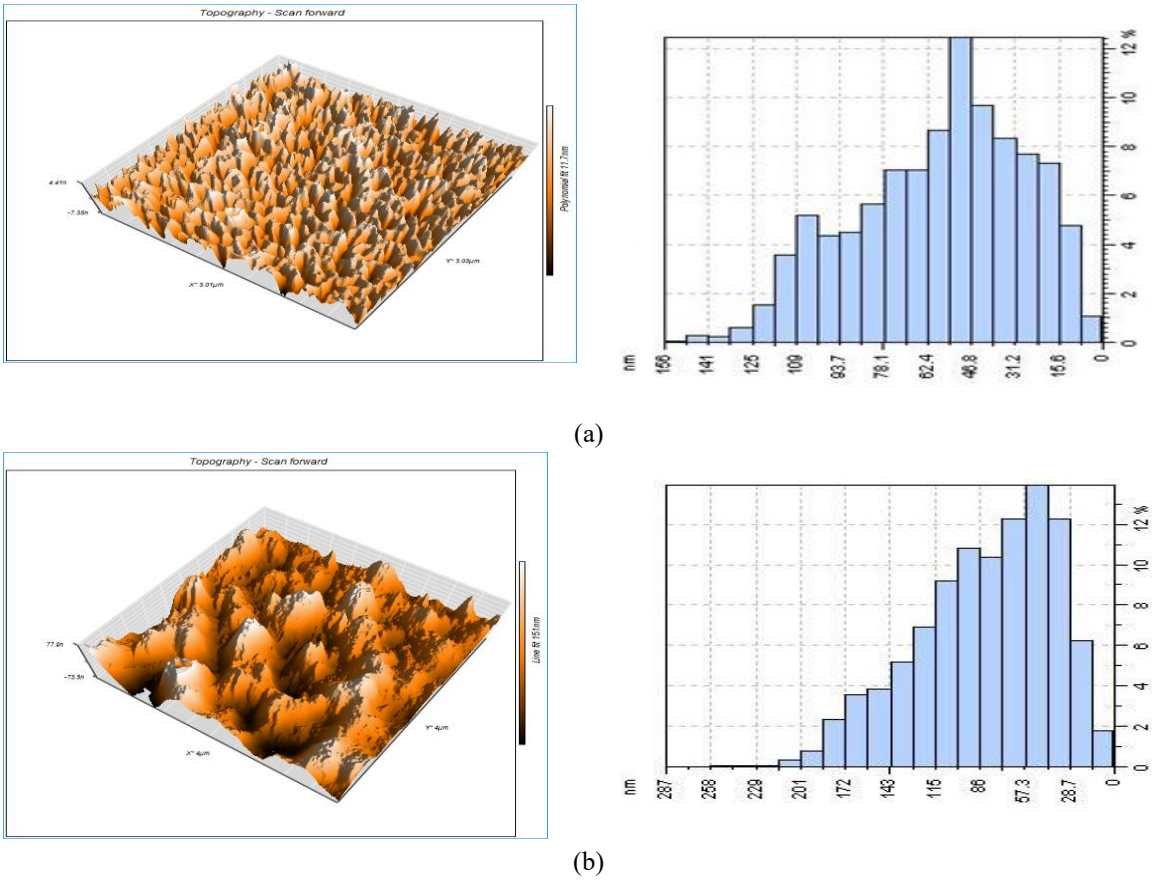

Figure 2. Morphology and size of (a) silica nanoparticles and (b) Silymarin-loaded silica nanoparticles using AFM

10.57647/ijic.2026.1701.06

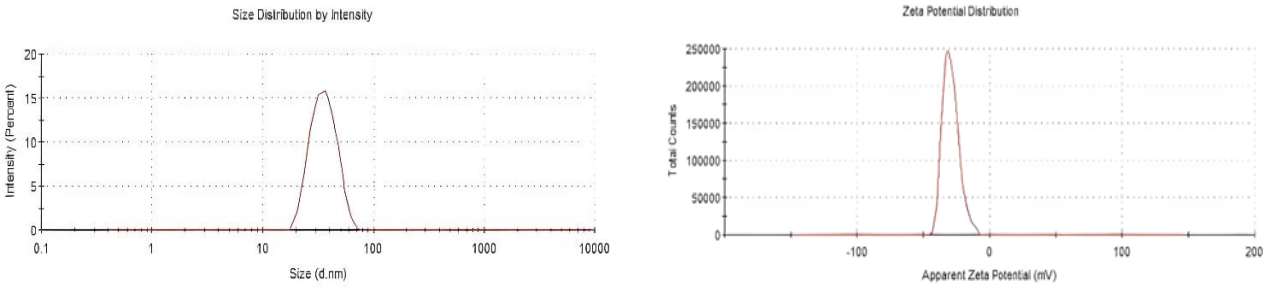

(a)

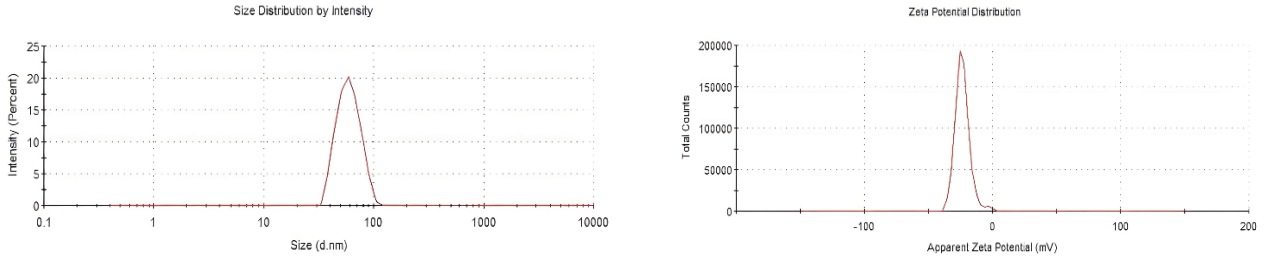

(b)

Figure 3. Size and zeta potential of a) silica nanoparticles and b) Silymarin-loaded nanoparticles using DLS

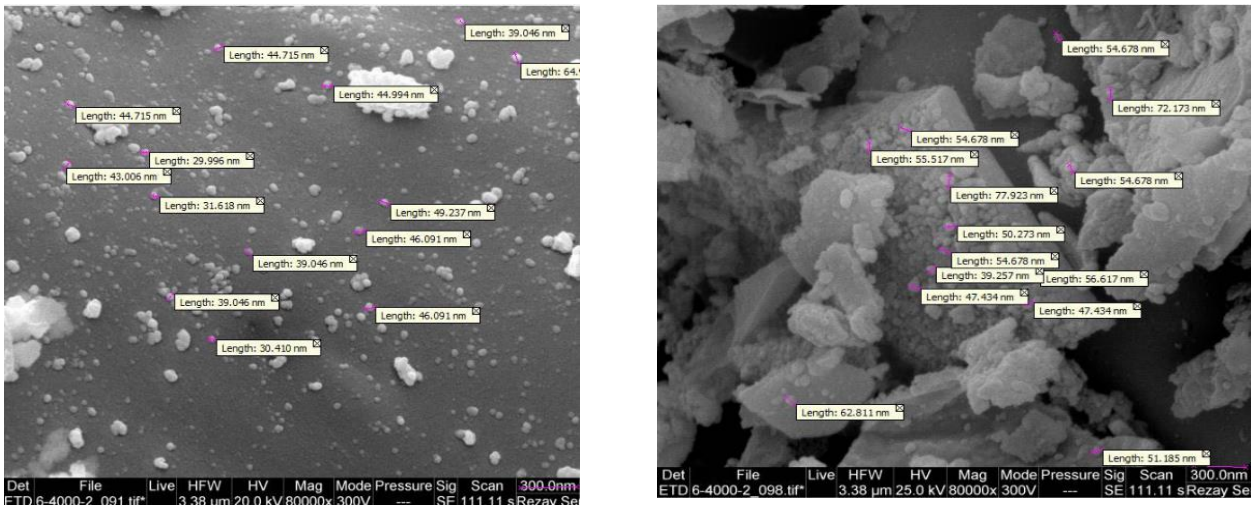

(a) (b)

Figure 4. Morphology and size of (a) silica nanoparticles (b) Silymarin-loaded nanoparticles

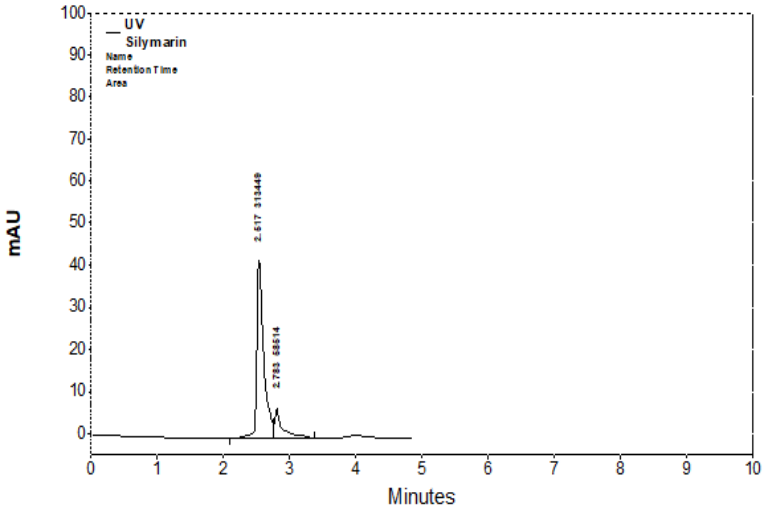

(a)

Figure 5. HPLC chromatograms of a) standard Silymarin (10 ppm) and b) Silymarin in the suspension (10 ppm)

10.57647/ijic.2026.1701.06

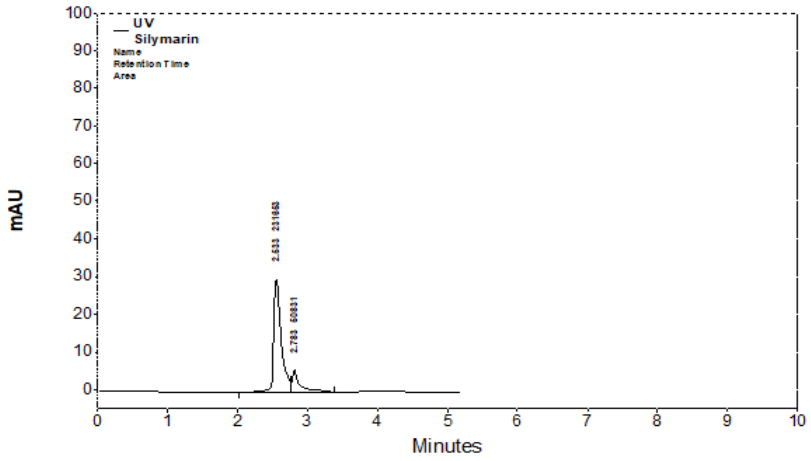

(b)

Figure 5. HPLC chromatograms of a) standard Silymarin (10 ppm) and b) Silymarin in the suspension (10 ppm)

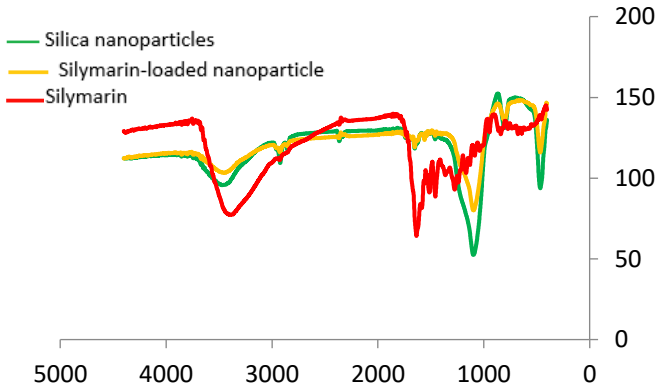

Figure 6. FTIR spectra of the synthesized silica nanoparticles, Silymarin-loaded nanoparticles and Silymarin

FTIR analysis was performed to determine the types of bonds present in the synthesized silica nanoparticles. Fig. 6 displays the FTIR spectra of the synthesized silica nanoparticles, Silymarin-loaded silica nanoparticles and Silymarin. In the spectrum shown in Fig. 6, the prominent peaks for silica are observed at 3527 cm^{-1}, 1095 cm^{-1}, and 469 cm^{-1}, corresponding to the asymmetric stretching bond O-Si-O and the bending bond O-Si, respectively [36, 37].

The prominent peaks for Silymarin are observed at 3402 cm^{-1} and 1636 cm^{-1}, as well as 1100 cm^{-1} and 459 cm^{-1}, representing the bonds O-H and C=C, respectively. Finally, the peaks attributed to Silymarin-loaded silica nanoparticles are shown at 3429cm^{-1}, 1647 cm^{-1}, 1100 cm^{-1}, and 1648 cm^{-1}. As evident in the FT-IR result, the ketone peak in the loading section is observed, and the intensity of the -OH peak in the 3429 cm^{-1} range has decreased. This reduction can be relied upon as evidence of loading [38].

3.4. Release of free and loaded Silymarin

Release profiles of free and loaded Silymarin in PBS (pH 7.4) and citric acid buffer (pH 5.5) are presented in Fig. 7. They show that silica nanoparticles enable slow and controlled drug release.

As observed, the release of free Silymarin is faster at pH 5.5 compared to pH 7.4, fully released within 4 h at pH 5.5 and taking 24 h at pH 7.4. These conditions hold for the Silymarin-loaded release as well. Silymarin loaded at pH 5.5 is fully released within 96 h, while at pH 7.4, it takes 120 h. In 2020, Maryam Montazeri et al. studied the Econazole release loaded in silica nanoparticles in the skin [39]. The results demonstrated an initial drug release of 80% within the first 8 h, followed by a continuous release over the next 24 h.

3.5. Toxicity study of synthesized silica nanoparticle using the MTT method

The cellular toxicity was assessed under laboratory conditions using the MTT method. For this purpose, four groups were selected: 1. Free Silymarin, 2. Silica nanoparticle, 3. Silymarin-loaded silica nanoparticle, and 4. Control. MCF-7 and Hep-G_2 cells were used as cancer cells, and fibroblast cells were used as normal cells. These cells were exposed to various concentrations of the studied groups for 24 and 48 h.

10.57647/ijic.2026.1701.06

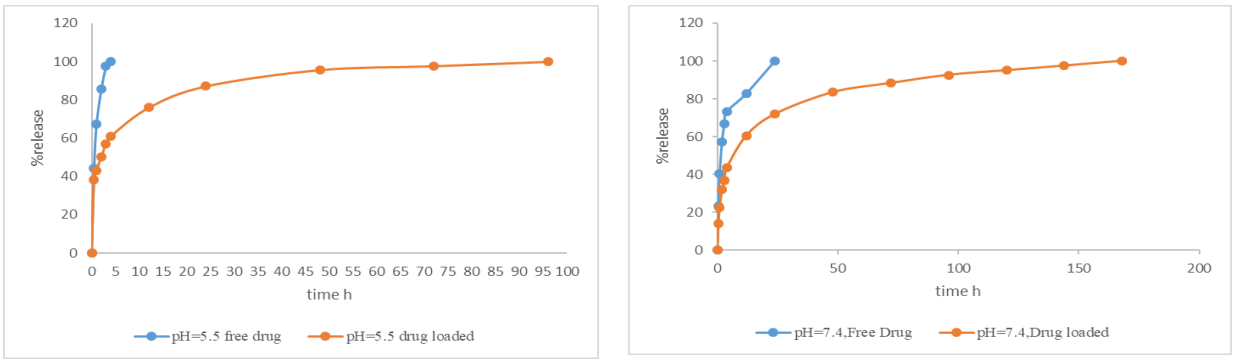

Figure 7. Release profiles of free and loaded Silymarin at pH 5.5 and 7.4

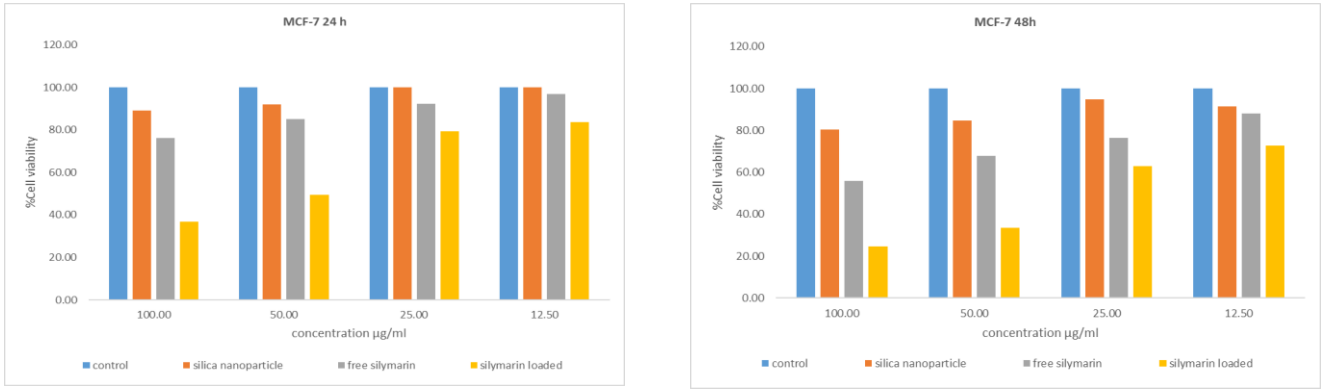

(a)

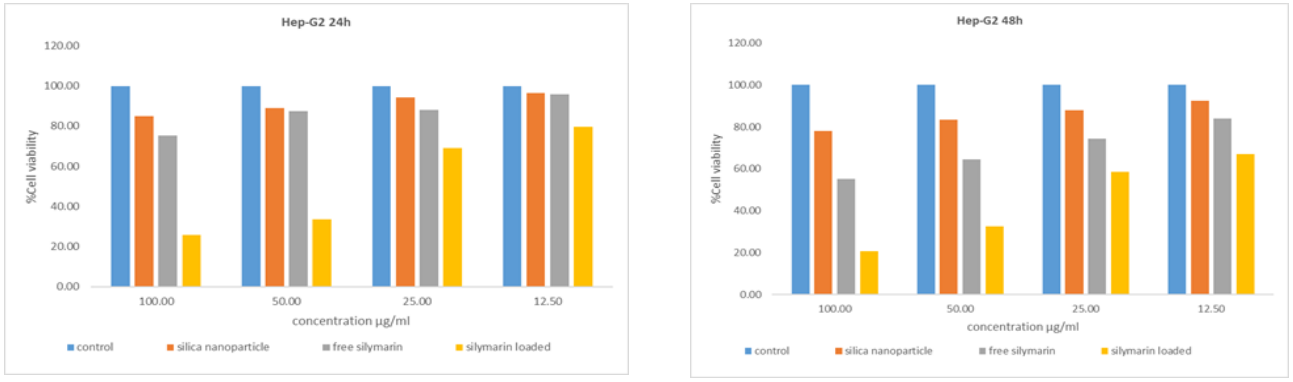

(b)

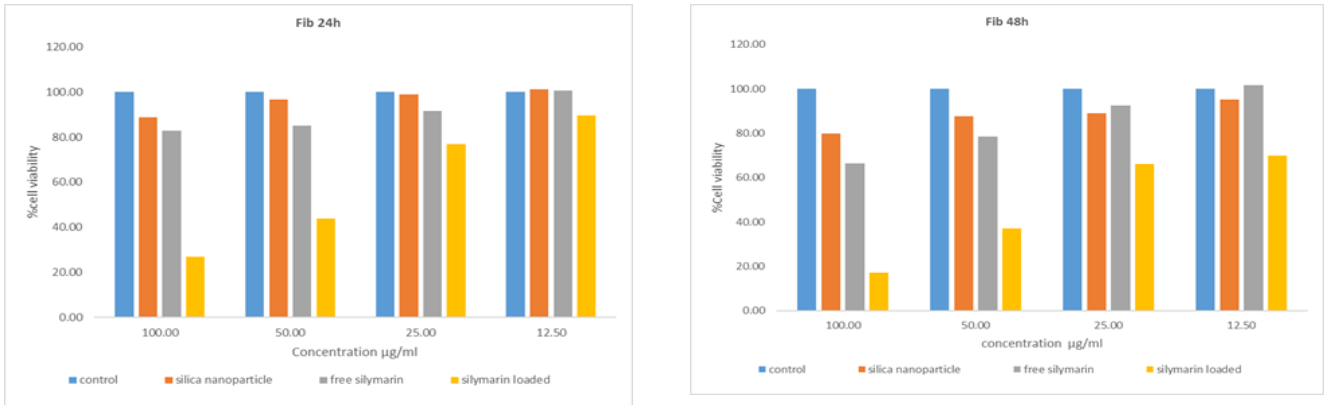

(c)

Figure 8. Cellular toxicity of the selected groups on (a) MCF-7, (b) Hep-G2 and (c) fibroblast cell line at 24 and 48 h

The cell survival rates of MCF-7, Hep-G2, and fibroblast cells are shown in Figs. 8 (a-c), respectively. In a study conducted by Aghapour et al. (2018), the effect of curcumin loading on silica nanoparticles on MCF-7 cancer cells were investigated [28]. Size of the synthesized silica nanoparticles using the thermal decomposition method was approximately 82 nm. MTT and apoptosis tests on MCF-7 cells were performed by

10.57647/ijic.2026.1701.06

comparing curcumin and curcumin loaded on silica nanoparticles at different concentrations (1-100 µM). The results showed that curcumin loaded on silica nanoparticles, compared to free curcumin, could more effectively reduce the activity, growth, and proliferation of breast cancer cells and induce apoptosis even at lower concentrations of curcumin [28].

4. Conclusion

This study represents the synthesis of silica nanoparticles from rice husk for controlled release of a poorly soluble Silymarin in order to develop its bioavailability. The prepared nanocarrier showed a quasi-spherical morphology and average particle size of approximately 55 nm. The in vitro release profiles of both free Silymarin and Silymarin-loaded silica nanoparticles reveal slow and controlled release of Silymarin. MTT assay shows reducing toxicity by encapsulation of Silymarin using silica nanoparticles. We believe our primary work would promote further study in clinical and in vivo research.

Authors Contribution
All the authors have participated sufficiently in the intellectual content, conception and design of this work or the analysis and interpretation of the data (when applicable), as well as the writing of the manuscript.

Availability of data and materials
The data that support the findings of this study are available from the corresponding author, upon reasonable request.

Conflict of interests
The author states that there is no conflict of interest.

References

[1] Desa S, Bhalani D, Jasoliya D, Punetha V, Modi Sh. D, Ray D, Aswal V. K, Pillai S. A, Comparative evaluation of Pluronic® micelles encapsulation efficiency for a diverse range of hydrophobic drugs: Implications for drug delivery, J Indian Chem Soc. 2025;102(5). https://doi.org/10.1016/j.jics.2025.101670

[2] Haseli M, Esmaeili A, A review of advances in coaxial Electrospinning for drug delivery, IJIC, 2023;14(1): 1-12. https://dx.doi.org/10.57647/j.ijic.2023.1401.03

[3] Rashidi L, Vasheghani farahani E, A review on the application of mesoporous silica nanoparticles as a drug delivery system, IJCCE, 2017;37(1):11-40.

[4] Narayan R, Nayak U, Raichur A, Garg S, Mesoporous Silica Nanoparticles: A Comprehensive Review on Synthesis and Recent Advances, Pharmaceutics. 2018;10(118). https://doi.org/10.3390/pharmaceutics10030118

[5] Galabova B.B, Mesoporous silica nanoparticles: Synthesis, functionalization, drug loading and release - A review. Trop J Pharm Res, 2021;20(5):1091-1100. http://dx.doi.org/10.4314/tjpr.v20i5.30

[6] Razavi-Nouri M. Jafarzadeh-Dogouri F, Oromiehie A, Ershad Langroudi A, Mechanical Properties and Water Absorption Behaviour of Chopped Rice Husk Filled Polypropylene Composites, Iran Polym J. 2006;15:757-766.

[7] Khamsehashari N, Hassanzadeh-Tabrizi S.A, Bigham A, Effects of strontium adding on the drug delivery behavior of silica nanoparticles synthesized by P123-assisted sol-gel method, Mater Chem Phys, 2018;205:283-291. https://doi.org/10.1016/j.matchemphys.2017.11.034

[8] Alhadhrami A, Gehad G.M, Ahmed H.S, Sameh H.I, Ebnalwaled A.A, Abdulraheem S.A.A, Behavior of Silica Nanoparticles Synthesized from Rice Husk Ash by the Sol–Gel Method as a Photocatalytic and Antibacterial Agent, Materials 2022;15:8211. https://doi.org/10.3390/ma15228211

[9] Awaji N, Ohkubo S, Nakanishi T, Aoyama T, Sugita Y, Takasaki K, Komiya S, Thermal oxide growth at chemical vapor deposited SiO2/Si interface during annealing evaluated by difference x-ray reflectivity, Appl. Phys. Lett. 1997;71:1954–1956. https://doi.org/10.1063/1.119753

[10] Park J.H, Oh C, Shin S.I, Moon S.K, Oh S.G, Preparation of hollow silica microspheres in W/O emulsions with polymers. J. Colloid. Interface Sci. 2003;266:107–114. https://doi.org/10.1016/s0021-9797(03)00645-3

[11] Wooldridge M.S, Torek P.V, Donovan M.T, Hall D.L, Miller T.A, Palmer T.R, Schrock C.R, An experimental investigation of gas-phase combustion synthesis of SiO2 nanoparticles using a multi-element diffusion flame burner, Combust. Flame. 2002;131:98–109. https://doi.org/10.1016/S0010-2180(02)00403-0

[12] Bonamartini A, Bondioli F, Maria A, Focher B, Leonelli C, Corradi A.B, Bondioli F, Ferrari A.M, Focher B, Leonelli C, Synthesis of silica nanoparticles in a continuous-flow microwave reactor, Powder Technol. 2006;167:45–48. https://doi.org/10.1016/j.powtec.2006.05.009

[13] Zarei V, Mirzaasadi M, Davarpanah A, Nasiri A, Valizadeh M, Sarbaz Hosseini M.J, Environmental Method for Synthesizing Amorphous Silica Oxide Nanoparticles from a Natural Material, Processes, 2021;9(2):334. https://doi.org/10.3390/pr9020334

[14] Fernandes I.J, Sánchez, F.A.L, Jurado J.R, Kieling A.G, Rocha T.L.A.C, Moraes C.A.M, Sousa V.C, Physical, chemical and electric characterization of thermally treated rice 5 husk ash and its potential application as ceramic raw material, Powder Technol, 2017;28:1228-1236. https://doi.org/10.1016/j.apt.2017.02.009

[15] Della V.P, Kuhn I, Hotza D, Rice husk ash as an alternate source for active silica production, Mater Lett, 2002;57:818–821. https://doi.org/10.1016/S0167-577X(02)00879-0

[16] Real C, Alcala MD, Criado JM, Preparation of silica from rice husks, J Am Ceram Soc, 1996;79(8):2012–2016. https://doi.org/10.1111/j.11512916.1996.tb08931.x

[17] Alshatwi AA, Athinarayanan J, Periasamy V.S, Biocompatibility assessment of rice husk-derived biogenic silica nanoparticles for biomedical applications, Mat Sci At Sci Eng C- Mater, 2015;47:8-16. https://doi.org/10.1016/j.msec.2014.11.005

[18] Paltinean G.A, Tomoaia G, Riga S, Mocanu A, Tomoaia-Cotisel M, Silymarin Based Complexes a mini Review, Academy of Romanian Scientists. 2022;11:146-166. https://doi.org/10.56082/annalsarscibio.2022.1.146

[19] Bijak M, Silybin A, Major Bioactive Component of Milk Thistle (Silybum marianum L. Gaernt.)- Chemistry, Bioavailability, and Metabolism, Molecules, 2017;22(11):1942. https://doi.org/10.3390/molecules22111942

[20] Lee D.Y.W, Liu Y, Molecular structure and stereochemistry of silybin A, silybin B, isosilybin A, and isosilybin B, isolated from silybum marianum (milk thistle), J. Nat. Prod. 2003;66(9):1171–1174.

[21] Liu C.H, Jassey A, Hsu H-Ya, Lin L-T, Antiviral Activities of Silymarin and Derivatives, Molecules. 1552;24: https://doi.org/10.3390/molecules24081552

[22] Sharifi-Rigi A, Heidarian E, Protective and anti-inflammatory effects of silymarin on paraquat-induced nephrotoxicity in rats, J. Herbmed. Pharmacol, 2019;8(1):28-34.

[23] Stiuso P, Scognamiglio I, Murolo M, Ferranti P, De Simone C, Rizzo M.R, Tuccillo C, Caraglia M, Loguercio C, Federico A, Serum oxidative stress markers and lipidomic profile to detect NASH patients responsive to an antioxidant treatment: a pilot study, Oxid. Med. Cellular. Longevity, 2014. https://doi.org/10.1155/2014/169216

[24] Theodosiou E, Purchartová K, Stamatis H, Kolisis F, Křen V, Bioavailability of silymarin flavonolignans: drug formulations and biotransformation, Phytochemistry reviews, 2013;13(1):1-18. https://doi.10.1007/s11101-013-9285-5

[25] Ghadi R, Dand N, BCS class IV drugs: highly notorious candidates for formulation development, J. Contr. Release, 2017;28(248):71–95. https://doi.10.1016/j.jconrel.2017.01.014

[26] Lee J-S, Hong D-Y, Kim E-S, Lee H-G, Improving the water solubility and antimicrobial activity of silymarin by nanoencapsulation Colloids and Surfaces, Biointerfaces, 2017;154. https://doi.org/10.1016/j.colsurfb.2017.03.004

[27] Nasr S.S, Nasra M.M.A, Hazzah H.A. Abdallah O.Y, Mesoporous silica nanoparticles, a safe option for silymarin delivery: preparation, characterization, and in vivo evaluation, Drug Deliv Transl Re, 2019;9(5):968-979.

[28] Aghapour F, Moghadamnia A.A , Nicolini A, Mousavi Kani S.N,Barari L, Morakabati P, Rezazadeh L, Kazemi S, Quercetin conjugated with silica nanoparticles inhibits tumor growthin MCF-7 breast cancer cell lines, Biochem Bioph Res Co, 2018;500(4):860-865. https://doi.org/10.1016/j.bbrc.2018.04.174

[29] Sankar S, Sharma SK, Kaur N, Lee B, Kim D.Y, Lee S, Biogenerated silica nanoparticles synthesized from sticky, red, and brown rice husk ashes by a chemical method, Ceram Int, 2016;42:4875-4885. https://doi.org/10.1016/j.ceramint.2015.11.172

[30] Das S, Roy P, Auddy R.G, Mukherjee A, Silymarin nanoparticle prevents paracetamol-induced hepatotoxicity, Int J Nanomed, 2011;6:1291-1301. https://doi.org/10.2147/IJN.S15160

[31] Cao X, Deng W, Fu M, Zhu Y, Liu H, Wang Li, Zeng J, Wei Y, Xu X, Yu J, Seventy-two-hour release formulation of the poorly soluble drug silybin based on porous silica nanoparticles: In vitro release kinetics and in vitro/in vivo correlations in beagle dogs, Eur J Pharm Sci, 2013;48(1-2):64-71. https://doi.10.1016/j.ejps.2012.10.012

[32] Owonubi S.J, Aderibigbe B.A, Mukwevho E, Sadiku E.R, Ray S.S, Characterization and in vitro release kinetics of antimalarials from whey protein-based hydrogel biocomposites, IJIC, 2018;9:39–52. https://doi.org/10.1007/s40090-018-0139-2

[33] Owonubi S.J, Mukwevho E, Aderibigbe B, Neerish Revaprasadu A, Sadiku E.R, Cytotoxicity and in vitro evaluation of whey protein-based hydrogels for diabetes mellitus treatment, IJIC, 2019;10:213–223. https://doi.org/10.1007/s40090-019-0185-4

[34] Mohammadi Sh, Khavarpour M, Ghadi A, Design of multiple-function matrix encapsulated with Marjoram extract to support cellular functions, stimulate collagen synthesis and decrease infection in wound, Sci Rep. 2024;14, https://doi.org/10.1038/s41598-024-71525-w

[35] Yuvakkumar R, ElangoV, Rajendran V, Kannan N, High-purity nano silica powder from rice husk using a simple chemical method, J. Exp. Nanosci. 2012;9:1-10. https://doi.org/10.1080/17458080.2012.656709

[36] Pijarn N, Jaroenworaluck A, Sunsaneeyametha W, Stevens R, Synthesis and characterization of nanosized-silica gels formed under controlled conditions, Powder Technol. 2010;203(2):462-468. https://doi.org/10.1016/j.powtec.2010.06.007

[37] Gangwar R.K, Tomar G.B, Dhumale V.A, Zinjarde S, Sharma R.B, Datar S, Curcumin conjugated silica nanoparticles for improving bioavailability and its anticancer applications, J Agr Food Chem, 2013;61:9632-9637. https://doi.org/10.1021/jf402894x

[38] Bui T.M.A, Nguyen T.V, Nguyen T.M, Hoang T.H, Nguyen T.T.H, Lai T.H, Tran T. N, Nguyen V.H, Hoang V.H, Le Tr.L, Tran D.L, Dang T.C, Vu Q.T, Nguyen-Tri Ph, Investigation of crosslinking, mechanical properties and weathering stability of acrylic polyurethane coating reinforced by SiO2 nanoparticles issued from rice husk ash, Mater Chem Phys, 2020;241:122445. https://doi.org/10.1016/j.matchemphys.2019.122445

[39] Montazeri M, Razzaghi-Abyaneh M, Nasrollahi S.A, Maibach H, Nafisi S, Enhanced topical econazole antifungal efficacy by amine-functionalized silica nanoparticles, Bull. Mater. Sci. 2020;43(13). https://doi.org/10.1007/s12034-019-1974-2